10.5005/jp-journals-10025-1018

ORIGINAL ARTICLE

Topometric and Tomographic Indices for the Diagnosis of Keratoconus

Fernando Faria Correia, Isaac Ramos, Bernardo Lopes, Marcella Q Salomão, Allan Luz, Rosane O Correa, Michael W Belin, Renato Ambrósio Jr

ABSTRACT

Purpose: To compare topometric (front surface curvature) and tomographic (3D corneal shape) indices for diagnosing keratoconus.

Methods: Pentacam data from one eye randomly selected of 200 normals (N) and 177 keratoconus (KC) were analyzed. Tomographic and topometric indices were tested. Receiver operating characteristic (ROC) curves were calculated, along with pairwise comparisons.

Results: All tested variables had significant differences among N and KC (Mann-Whitney, $p < 0.001$). Most accurate tomographic indices had higher AUC than best topometric ones (DeLong, $p < 0.05$). Belin-Ambrosio D (BAD-D) had AUC of 1.00 (sensitivity 100.0%; specificity 98.5%).

Conclusion: Tomographic data was superior than topometric data to detect keratoconus. The BAD-D was an enhanced approach for detecting keratoconus.

Keywords: Keratoconus, Corneal topography, Corneal tomography, Diagnosis.

How to cite this article: Correia FF, Ramos I, Lopes B, Salomão MQ, Luz A, Correa RO, Belin MW, Ambrósio R Jr. Topometric and Tomographic Indices for the Diagnosis of Keratoconus. Int J Kerat Ect Cor Dis 2012;1(2):92-99.

Source of support: Nil

Conflict of interest: None

INTRODUCTION

Keratoconus is a bilateral noninflammatory ectatic disease, characterized by progressive thinning and protrusion of the cornea.[1,2] In the past, the diagnosis of this disease was based on clinical findings and typical slit-lamp signs (i.e. Fleischer ring, Vogt striae, Munson sign or Rizzuti sign).[1,2] Although, advanced keratoconus is easily identified with slit-lamp biomicroscopic examination or keratometry, mild forms of keratoconus may be overlooked. In the early 1900s, Mark Amsler described early forms of keratoconus without clinical signs using photokeratoscopy.[3] Only in the mid-1980s, Stephen D Klyce, developed algorithms for surface reconstruction of the acquired reflection image from Placido-based videokeratoscopy, allowing color-coded maps and quantitative data of the front surface of the cornea.[4] To assist the diagnosis of mild forms of ectasia, indices and methods based on corneal topography were designed. The accuracy of these methods was demonstrated in several studies.[5-9] Thereby, corneal topography represented a true revolution in the diagnosis and management of corneal disease.[5-7] One of the most important applications was in refractive surgical screening, as well as evaluating and improving the results of corneal surgical procedures.[10-14]

Other technologies were a further improvement in corneal imaging.[15-20] The Pentacam (Oculus Optikgeräte GmbH, Wetzlar, Germany) is an anterior segment tomography device, based on a rotating Scheimpflug camera. Corneal tomography has the ability to measure not only the anterior corneal surface but also the posterior surface, allowing a three-dimensional image of the cornea. This technology provides significantly more information than anterior surface topography, as tomography utilizes data from anterior and posterior surfaces of the cornea, as well as pachymetric mapping.[21-24]

The goal of this study was to determine and compare the accuracy of anterior surface curvature, front and back elevation, pachymetric and combined tomographic-derived indices for discriminating clinical keratoconus from normal corneas.

METHODS

The retrospective study adhered to the tenets of the Declaration of Helsinki and was approved by the ethics committee of the Federal University of São Paulo, Brazil. Patients examined at the Instituto de Olhos Renato Ambrósio (Rio de Janeiro, Brazil) were retrospectively enrolled. Data was analyzed at the Rio de Janeiro corneal tomography and biomechanics study group.

One eye randomly selected from 177 consecutive patients with clinical bilateral keratoconus (KC) were retrospectively enrolled (group KC). Control group included one eye randomly selected from 200 age-matched patients selected from a database of normal (N) patients considered as good candidates (group N).

Along with a comprehensive ocular examination, all eyes were examined by at least one Placido-disk-based corneal topography system (Keratograph Topography System [Oculus, Wetzlar, Germany], Atlas [Carl Zeiss, Jena, Germany]; iTrace [Tracey Technologies, Houston, US]) and rotating Scheimpflug corneal tomography (Pentacam HR). Diagnosis of keratoconus was made based on criteria used in the collaborative longitudinal evaluation of keratoconus (CLEK) study.[25]

Keratoconus cases with a history of corneal surgery or with extensive corneal scarring were excluded from the

study. Contact lenses were discontinued at least 3 weeks prior to the Pentacam examination. During the Pentacam examination, the patient was comfortably positioned at the instrument with proper placement on the chin rest and forehead strap. The patient was asked to blink a couple of times and to open both eyes and stare at the fixation target. After proper alignment was obtained, the automatic release mode started the scan using 25 single Scheimpflug images captured within 2 seconds for each eye. Only cases with acceptable quality images were included in the study. The Pentacam software (1.17b145) was used to automatically extract the data from each examination into a Microsoft Excel (Microsoft, Redmond, Washington) spreadsheet.

The following front surface derived curvature indices were analyzed: Steepest or maximal keratometry (Kmax); index of surface variance (ISV); index of vertical asymmetry (IVA); index of highest asymmetry; index of highest decentration (IHD); front surface asphericity (Asph Q front 30º). The oculus topographic keratoconus classification (TKC) was assessed.[26] The elevation parameters derived from the front and back surfaces at the apex, at the thinnest point and the point with highest value within the 4 mm (diameter) zone centered at the apex were calculated using the 8 mm best-fit sphere (BFS) and 8 mm best-fit toric ellipsoid (BFTE) references were computed.

Corneal thickness at the apex (central value – Pachy apex) and at the thinnest point (Pachy min); pachymetric progression index at the meridian with maximal pachymetric increase (PPI max) and the average of all meridians (PPI avg); and the relational thickness to these parameters (ART avg and ART max) were registered. The Belin/Ambrósio enhanced ectasia display (BAD) deviation indices were computed along with the BAD-D value which combines these indices based on a linear regression analysis.

Statistical analysis was accomplished using BioEstat 5.0 (Instituto Mamirauá, Amazonas, Brazil) and Med-Calc 11.1 (MedCalc Software, Mariakerke, Belgium). Nonparametric Mann-Whitney U-test (Wilcoxon rank sum test) was used for assessing whether each variable had different distributions among the groups. Receiver operating characteristic (ROC) curves were calculated for all parameters to provide the best cutoff value for optimizing sensitivity and specificity for the diagnosis of keratoconus and to determine the test's overall predictive accuracy and area under the curve. Pairwise comparisons of the ROC curves were performed to test whether significant differences were present between the areas from each parameter using DeLong method. A p-value < 0.05 was considered statistically significant.

RESULTS

Average patient age was 33.04 ± 11.96 years (range: 11.70 -65.20 years) and 30.95 ± 11.38 years (range: 8.02-67.39 years) in the normal and keratoconic groups respectively. There was no statistical difference for patient age between the groups (Mann-Whitney U-test; p = 0.3281). The percentages of male/female were 49.72/50.28 and 41.95/58.05 in the normal and keratoconic groups respectively. Accordingly to the Krumeich-Amlser classification of the severity of keratoconus, there were 42 eyes (23.73%) classified as grade I, 74 eyes (41.81%) classified as grade II and 43 eyes (24.29%) classified as grade III.

Oculus TKC system (based on anterior surface indices) failed to identify 18 eyes (10.17%) with clinical diagnosis keratoconus. Figure 1 shows the sagittal (axial) curvature

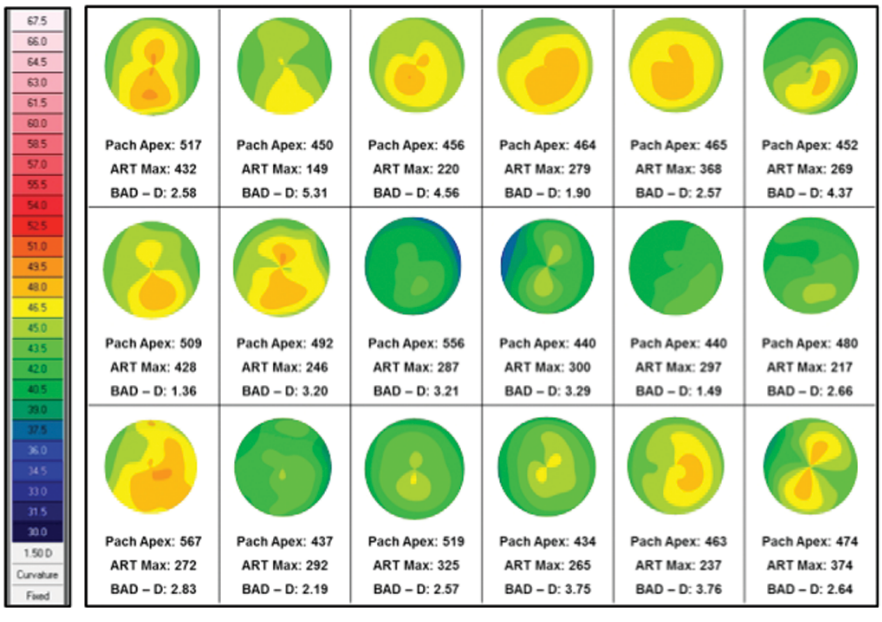

Fig. 1: Sagittal curvature map (using Klyce-Smolek color scale), thickness at the apex and combined tomographic parameters of keratoconus eyes which were not identified by the anterior surface-derived indices

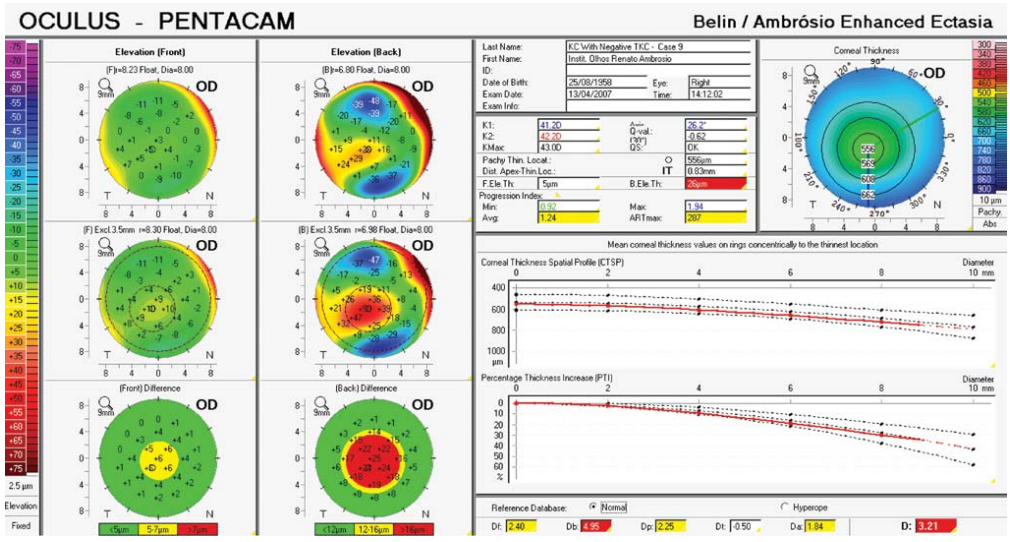

Fig. 2: BAD display of keratoconus case with negative TKC

maps along with thickness parameters (Pachy apex and ART max) and the BAD-D value of these eyes. Figure 2 shows the BAD display of one keratoconus eye with negative TKC.

Mean, median and range of Pentacam parameters are displayed in Table 1. There were statistically significant differences between normal and keratoconic groups for all parameters (Mann-Whitney U-test, $p < 0.001$).

Table 2 displays the best cutoffs for optimizing sensitivity and specificity to separate the two study populations (KC and N), the area under the ROC curve (AUC), standard error (SE), 95% confidence interval (CI), and significance level for each parameter tested.

Regarding the anterior surface curvature data, ISV and IHD parameters performed statistically better than the other topometric variables ($p < 0.05$) in the pairwise comparison of the ROC curves (Table 3). No statistically significant differences were noted between the ROC curves obtained from ISV, IHD and Kmax ($p > 0.05$). Asph front Q (30º) variable performed significantly worse than all the other anterior surface-derived parameters ($p < 0.05$).

The elevation values at the thinnest point had better performances of either front and back surfaces using both BFS and BFTE. Posterior elevation (Ele B BFS 8 mm thinnest and Ele B BFTE 8 mm thinnest) derived parameters had the highest AUC, 0.983 and 0.986, respectively. In the pairwise comparison of the ROC curves (Table 4), there were no significant differences between the performance of Ele B BFS 8 mm thinnest and Ele B BFTE 8 mm thinnest parameters ($p = 0.32$).

Pachy apex had a lower area under the curve than Pachy min (0.921 *vs* 0.947, $p < 0.001$). PPI avg, PPI max and the relational thickness of the thinnest value to these parameters (ART avg and ART max) had statistically better AUC than Pachy min and Pachy apex ($p < 0.05$; Table 5).

Pairwise comparisons of the ROC curves of BAD-D parameter and its derived indices are displayed in Table 6. No statistically significant differences were noted between the ROC curves obtained from BAD-D, BAD-Daa, BAD-Dam and BAD-Dp ($p > 0.05$).

The best parameters for discriminating keratoconus were BAD-D, ART avg and ART max: BAD-D had area under the curve of 1.000 (95% CI: 0.989 – 1.000); ART avg had area under the curve of 0.997 (95% CI: 0.985 – 1.000); ART-max had area under the curve of 0.997 (95% CI: 0.985 – 1.000).

Table 7 shows the pairwise comparisons of the ROC curves of the best topometric, tomographic and combined parameters. No statistically significant differences were noted between the ROC curves obtained from BAD-D and the relational thickness parameters (ART avg and ART max). Ele B BFTE 8 mm thinnest had not statistically significant differences compared to the relational thickness indices. Figure 3 displays the ROC curves of the best topometric, tomographic and combined parameters.

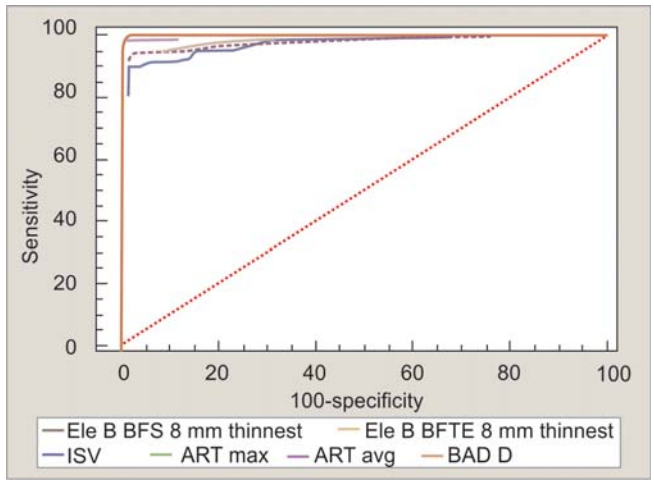

Fig. 3: ROC curves of the best topometric, tomographic and combined parameters

Table 1: Pentacam parameters measured in normal and keratoconic eyes

	Normal					*KC*					*p-value*
	Mean	*Median*	*SD*	*Min*	*Max*	*Mean*	*Median*	*SD*	*Min*	*Max*	
ISV	20.61	19.00	6.39	8.00	47.00	79.76	20.00	38.90	17.00	199.00	<0.001
IVA	0.18	0.17	0.07	0.04	0.38	0.85	0.78	0.45	0.04	2.17	<0.001
IHA	4.25	3.40	3.35	0.10	15.50	25.09	22.40	19.94	0.10	112.70	<0.001
IHD	0.01	0.01	0.00	0.00	0.03	0.07	0.06	0.05	0.01	0.26	<0.001
K_{max} front	44.57	44.60	1.50	40.80	48.80	54.00	52.50	6.92	43.00	86.10	<0.001
Asph. Q front (30°)	–0.27	–0.26	0.12	0.06	–0.67	–0.67	–0.61	0.49	0.59	–2.32	<0.001
Ele F BFS 8 mm apex	1.74	2.00	1.18	–2.00	6.00	8.85	6.00	9.54	–5.00	65.00	<0.001
Ele F BFS 8 mm max 4 mm zone	6.46	6.00	2.87	2.00	19.00	26.85	26.00	13.94	3.00	71.00	<0.001
Ele F BFS 8 mm thinnest	1.57	2.00	2.04	–6.00	7.00	22.00	20.00	13.32	–6.00	70.00	<0.001
Ele B BFS 8 mm apex	1.75	1.00	2.81	–5.00	12.00	18.69	13.00	22.61	–19.00	182.00	<0.001
Ele B BFS 8 mm max 4 mm zone	13.01	13.00	4.38	4.00	26.00	54.08	48.00	28.27	8.00	189.00	<0.001
Ele B BFS 8 mm thinnest	3.55	3.00	4.18	–4.00	16.00	48.86	43.00	29.30	2.00	189.00	<0.001
Ele F BFTE 8 mm apex	–0.25	0.00	1.42	–5.00	6.00	7.84	6.00	9.90	–8.00	63.00	<0.001
Ele F BFTE 8 mm max 4 mm zone	2.77	2.00	1.32	1.00	8.00	16.86	15.00	10.94	1.00	65.00	<0.001
Ele F BFTE 8 mm thinnest	–0.46	0.00	1.50	–6.00	5.00	14.34	13.00	10.63	–1.00	51.00	<0.001
Ele B BFTE 8 mm apex	–0.14	–1.00	3.81	–9.00	14.00	18.02	12.00	23.64	–30.00	163.00	<0.001
Ele B BFTE 8 mm max 4 mm zone	7.33	7.00	2.53	2.00	16.00	42.06	37.00	26.95	4.00	206.00	<0.001
Ele B BFTE 8 mm thinnest	–0.01	0.00	3.60	–10.00	12.00	39.18	33.00	26.94	–2.00	185.00	<0.001
Pachy min	549.23	547.00	35.47	454.00	660.00	459.06	464.00	47.60	296.00	568.00	<0.001
Pachy apex	552.28	550.00	35.93	458.00	665.00	474.40	475.00	45.54	306.00	584.00	<0.001
RPI max	1.07	1.06	0.16	0.63	2.07	2.99	2.43	1.86	1.19	14.95	<0.001
RPI avg	0.85	0.85	0.11	0.60	1.28	2.12	1.77	1.31	0.88	10.78	<0.001
ART max	526.69	513.00	90.64	219.00	908.00	192.99	193.00	83.28	21.00	432.00	<0.001
ART avg	655.99	646.00	103.97	354.00	999.00	265.90	264.00	106.29	28.00	550.00	<0.001
BAD Df	0.07	–0.06	1.09	–1.62	4.10	9.30	7.27	7.50	–1.63	48.45	<0.001
BAD Db	–0.13	–0.41	0.96	–1.48	3.35	7.05	5.78	6.21	–1.31	43.94	<0.001
BAD Dp	–0.35	–0.39	0.72	–2.08	2.56	8.24	5.86	8.88	–0.15	66.78	<0.001
BAD Dt	–0.26	–0.26	0.97	–2.86	2.84	2.86	2.46	2.13	–0.82	12.62	<0.001
BAD Dy	0.37	0.38	1.08	–3.17	3.74	1.68	1.60	1.58	–3.00	8.24	<0.001
BAD De	–0.17	–0.34	0.89	–1.83	2.48	9.56	8.24	6.30	–0.45	39.69	<0.001
BAD Dam	–0.35	–0.22	0.83	–3.84	2.46	2.70	2.70	0.76	0.51	4.27	<0.001
BAD Daa	–0.32	–0.24	0.78	–2.90	1.96	2.62	2.64	0.80	0.48	4.41	<0.001
BAD Dk	–0.26	–0.26	0.93	–2.61	2.38	5.60	4.66	4.30	–1.22	25.56	<0.001
BAD Dr	–0.04	–0.30	1.13	–1.72	4.69	3.16	2.44	3.40	–1.52	19.07	<0.001
BAD D	0.43	0.43	0.57	–1.20	2.71	8.08	7.14	4.99	1.36	33.93	<0.001

ISV: Index of surface variance; IVA: Index of vertical asymmetry; IHA: Index of highest asymmetry; IHD: Index of highest decentration; K_{max} front: Steepest keratometry; Asph Q front (30º): Front surface asphericity; Ele F BFS 8 mm apex: Front surface elevation at the apex using the 8 mm best-fit sphere; Ele F BFS 8 mm max 4 mm zone: Front surface elevation at the point with highest value within the 4 mm (diameter) zone centered at the apex using the 8 mm best-fit sphere; Ele F BFS 8 mm thinnest: Front surface elevation at the thinnest point using the 8 mm best-fit sphere; Ele B BFS 8 mm apex: Back surface elevation at the apex using the 8 mm best-fit sphere; Ele B BFS 8 mm max 4 mm zone: Back surface elevation at the point with highest value within the 4 mm (diameter) zone centered at the apex using the 8 mm best-fit sphere; Ele B BFS 8 mm thinnest: Back surface elevation at the thinnest point using the 8 mm best-fit sphere; Ele F BFTE 8 mm apex: Front surface elevation at the apex using the 8 mm best-fit toric ellipsoid; Ele F BFTE 8 mm max 4 mm zone: Front surface elevation at the point with highest value within the 4 mm (diameter) zone centered at the apex using the 8 mm best-fit toric ellipsoid; Ele F BFTE 8 mm thinnest: Front surface elevation at the thinnest point using the 8 mm best-fit toric ellipsoid; Ele B BFTE 8 mm apex: Back surface elevation at the apex using the 8 mm best-fit toric ellipsoid; Ele B BFTE 8 mm max 4 mm zone: Back surface elevation at the point with highest value within the 4 mm (diameter) zone centered at the apex using the 8 mm best-fit toric ellipsoid; Ele B BFTE 8 mm thinnest: Back surface elevation at the thinnest point using the 8 mm best-fit toric ellipsoid; Pachy min: Corneal thickness at the thinnest point; Pachy apex: Corneal thickness at the apex; RPI max: Maximum pachymetric progression index; RPI avg: Average pachymetric progression index; ART max: Ambrósio relational thickness maximum; ART avg: Ambrósio relational thickness average; BAD Df: Deviation of front elevation difference map; BAD Db: Deviation of front elevation difference map; BAD Dp: Deviation of average pachymetric progression; BAD Dt: Deviation of minimum thickness; BAD Dy: Deviation from the vertical displacement of the thinnest point from the apex; BAD De: Deviation from the posterior elevation at the thinnest point considering BFS 8 mm; BAD Dam: Deviation of ART max; BAD Daa: Deviation of ART avg; BAD Dk: Deviation from Kmax; BAD Dr: Deviation from the more negative value on the relative thickness map; BAD D: Belin/Ambrósio enhanced ectasia total deviation value

DISCUSSION

Topometric indices derived from the front surface curvature of the cornea were analyzed in this study. Previous reports demonstrated similar results for diagnosing keratoconus between these parameters and indices based on videokeratoscopy (Ambrósio unpublished data 2009, 2010 and 2011; Belin unpublished data 2009). Anterior surface curvature (T) derived parameters provided by the Pentacam comprehensive eye scanner were accurate for discriminating keratoconus from normal eyes. According to the AUC analysis, the best anterior surface curvature derived variables were the ISV and the IHD (0.977 and 0.974 respectively). The concepts of these topometric indices are similar to the I-S value methodology proposed by Rabinowitz (Ambrósio

Table 2: Data summary from ROC curves of Pentacam parameters in normal and keratoconic eyes

Parameter	*Cut-off*	*AUC*	*Sensitivity*	*Specificity*	*SE*	*95% CI*	*p-value*
ISV	>35	0.977	90.4	98.0	0.00815	0.956 - 0.989	0.0001
IHA	>10.1	0.89	72.3	95.6	0.0176	0.854 - 0.919	0.0001
IVA	>0.32	0.958	87.6	97.6	0.0109	0.933 - 0.976	0.0001
IHD	>0.021	0.974	89.3	98.5	0.00867	0.952 - 0.987	0.0001
K_{max}	>47.4	0.972	91.0	96.6	0.00898	0.950 - 0.986	0.0001
Asph Q front (30º)	≤-0.45	0.801	66.1	90.7	0.0223	0.758 - 0.840	0.0001
Ele F BFS 8 mm apex	>3	0.836	70.1	94.6	0.0212	0.795 - 0.871	0.0001
Ele F BFS 8 mm max 4 mm zone	>12	0.958	87.6	96.6	0.011	0.932 - 0.975	0.0001
Ele F BFS 8 mm thinnest	>5	0.973	91.5	99.0	0.00871	0.952 - 0.987	0.0001
Ele F BFTE 8 mm apex	>1	0.857	75.1	95.2	0.0199	0.818 - 0.891	0.0001
Ele F BFTE 8 mm max 4 mm zone	>5	0.954	87.0	96.1	0.0114	0.928 - 0.973	0.0001
Ele F BFTE 8 mm thinnest	>2	0.968	89.8	99.5	0.00961	0.945 - 0.983	0.0001
Ele B BFS 8 mm apex	>6	0.857	72.3	92.7	0.0199	0.818 - 0.890	0.0001
Ele B BFS 8 mm max 4 mm zone	>22	0.976	92.7	97.1	0.00835	0.955 - 0.989	0.0001
Ele B BFS 8 mm thinnest	>12	0.983	94.4	97.6	0.00704	0.964 - 0.993	0.0001
Ele B BFTE 8 mm apex	>3	0.854	79.1	84.9	0.0201	0.814 - 0.888	0.0001
Ele B BFTE 8 mm max 4 mm zone	>14	0.972	90.4	99.0	0.00896	0.950 - 0.986	0.0001
Ele B BFTE 8 mm thinnest	>7	0.986	93.8	97.6	0.00622	0.969 - 0.995	0.0001
Pachy apex	≤517	0.921	85.9	84.9	0.0142	0.889 - 0.946	0.0001
Pachy min	≤496	0.947	81.9	95.1	0.0116	0.919 - 0.967	0.0001
RPI avg	>1.05	0.995	97.7	98.5	0.00386	0.981 - 0.999	0.0001
RPI max	>1.42	0.995	95.5	95.5	0.00394	0.981 - 0.999	0.0001
ART avg	≤474	0.997	98.3	99	0.00254	0.985 - 1.000	0.0001
ART max	≤496	0.997	98.9	99	0.00273	0.985 - 1.000	0.0001
BAD Daa	>0.96	0.997	98.3	99	0.00273	0.985 - 1.000	0.0001
BAD Dam	>0.78	0.997	98.9	99	0.00293	0.985 - 1.000	0.0001
BAD Db	>1.5	0.967	91.5	92.2	0.00976	0.943 - 0.982	0.0001
BAD De	>1.7	0.983	94.4	97.6	0.00703	0.964 - 0.993	0.0001
BAD Df	>2.16	0.966	92.7	94.6	0.0099	0.942 - 0.981	0.0001
BAD Dk	>1.49	0.972	91	96.6	0.000896	0.950 - 0.986	0.0001
BAD Dp	>0.91	0.995	98.3	98.6	0.0038	0.981 - 0.999	0.0001
BAD Dr	>0.36	0.885	87.6	76.6	0.018	0.848 - 0.915	0.0001
BAD Dt	>1.28	0.947	81.92	95.12	0.0123	0.919 - 0.967	0.0001
BAD Dy	>0.74	0.766	73.4	69.8	0.0246	0.720 - 0.808	0.0001
BAD D	>1.34	1	100.0	98.5	0.000112	0.989 - 1.000	0.0001

ISV: Index of surface variance; IVA: Index of vertical asymmetry; IHA: Index of highest asymmetry; IHD: Index of highest decentration; K_{max} front: Steepest keratometry; Asph Q front (30º): Front surface asphericity; Ele F BFS 8 mm apex: Front surface elevation at the apex using the 8 mm best-fit sphere; Ele F BFS 8 mm max. 4 mm zone: Front surface elevation at the point with highest value within the 4 mm (diameter) zone centered at the apex using the 8 mm best-fit sphere; Ele F BFS 8 mm thinnest: Front surface elevation at the thinnest point using the 8 mm best-fit sphere; Ele B BFS 8 mm apex: Back surface elevation at the apex using the 8 mm best-fit sphere; Ele B BFS 8 mm max 4 mm zone: Back surface elevation at the point with highest value within the 4 mm (diameter) zone centered at the apex using the 8 mm best-fit sphere; Ele B BFS 8 mm thinnest: Back surface elevation at the thinnest point using the 8 mm best-fit sphere; Ele F BFTE 8 mm apex: Front surface elevation at the apex using the 8 mm best-fit toric ellipsoid; Ele F BFTE 8 mm max 4 mm zone: Front surface elevation at the point with highest value within the 4 mm (diameter) zone centered at the apex using the 8 mm best-fit toric ellipsoid; Ele F BFTE 8 mm thinnest: Front surface elevation at the thinnest point using the 8 mm best-fit toric ellipsoid; Ele B BFTE 8 mm apex: Back surface elevation at the apex using the 8 mm best-fit toric ellipsoid; Ele B BFTE 8 mm max 4 mm zone: Back surface elevation at the point with highest value within the 4 mm (diameter) zone centered at the apex using the 8 mm best-fit toric ellipsoid; Ele B BFTE 8 mm thinnest: Back surface elevation at the thinnest point using the 8 mm best-fit toric ellipsoid; Pachy min: Corneal thickness at the thinnest point; Pachy apex: Corneal thickness at the apex; RPI max.: Maximum pachymetric progression index; RPI avg: Average pachymetric progression index; ART max: Ambrósio relational thickness maximum; ART avg: Ambrósio relational thickness average; BAD Df: Deviation of front elevation difference map; BAD Db: Deviation of front elevation difference map; BAD Dp: Deviation of average pachymetric progression; BAD Dt: Deviation of minimum thickness; BAD Dy: Deviation from the vertical displacement of the thinnest point from the apex; BAD De: Deviation from the posterior elevation at the thinnest point considering BFS 8 mm; BAD Dam: Deviation of ART max; BAD Daa: Deviation of ART avg; BAD Dk: Deviation from K_{max}; BAD Dr: Deviation from the more negative value on the relative thickness map; BAD D: Belin/Ambrósio enhanced ectasia total deviation value

unpublished data 2009, 2010 and 2011; Belin unpublished data 2009).

Eighteen keratoconus eyes (10.17%) were not identified by the topometric indices analysis provided by the device. When the ectatic change is not yet present on the front surface, corneal topography can be normal despite subtle disease. Although these variables may be used as objective parameters to detect keratoconus, this finding enhances the idea that they may lead to relatively later identification of ectasia, with lower sensitivity than tomographic indices.[27-29] Regarding tomographic data, all 18 eyes have BAD – D > 1.34 and ART max < 496.

Elevation-based tomographic data is a complex matter and its interpretation can be challenging. Michael W Belin, has proposed methods for an easier elevation analysis, introducing the reference surface concept. Elevation maps represent the difference from the examined corneal surface (anterior or posterior) compared with a chosen reference body.

Different geometric bodies can be used as reference for the elevation map, such as spheres and toric ellipsoids.[24, 30] According to the AUC analysis, the best elevation parameters were the back surface elevation at the thinnest point using 8 mm BFS and 8 mm BFTE (0.983 and 0.986, respectively). Interestingly, we found similar performances for these parameters ($p > 0.05$). The pairwise comparison of the area under the curve for back and front elevation at the thinnest point showed no statistical difference, except for the comparison of back and front elevation using 8 mm BFTE ($p = 0.035$). Such difference is explained by the impact of different reference bodies in the elevation display: BFTE reference body has a better adaptation to the corneal astigmatism component, showing less sensitivity to highlight ectasia.

Table 3: Pair-wise comparison of the AUC for anterior surface curvature-derived parameters

	ISV	*IHA*	*IVA*	*IHD*	*Asph Q front (30°)*
K_{max} front	0.611	<0.001	0.302	0.858	<0.001
ISV		<0.001	0.034	0.691	<0.001
IHA			<0.001	<0.001	0.001
IVA				0.039	<0.001
IHD					<0.001

ISV: Index of surface variance; IVA: Index of vertical asymmetry; IHA: Index of highest asymmetry; IHD: Index of highest decentration; K_{max} front: Steepest keratometry; Asph Q front (30º): Front surface asphericity; De Long method

Table 5: Pair-wise comparison of the AUC for thickness derived parameters

	Pachy min	*RPI avg*	*RPI max*	*ART avg*	*ART max*
Pachy apex	<0.001	<0.001	<0.001	<0.001	<0.001
Pachy min		<0.001	<0.001	<0.001	<0.001
RPI avg			0.925	0.159	0.353
RPI max				0.319	0.173
ART avg					0.796

Pachy min: Corneal thickness at the thinnest point; Pachy apex: Corneal thickness at the apex; RPI max.: Maximum pachymetric progression index; RPI avg: Average pachymetric progression index; ART max: Ambrósio relational thickness maximum; ART avg: Ambrósio relational thickness average; De Long method

Tomographic relational thickness metrics had statistically better diagnostic performances than single-point values to identify keratoconus. However, no statistically significant differences were noted in the pairwise comparisons of the AUC among PPI ave, PPI max, and the relational thickness to these parameters.

The best parameter for diagnosing keratoconus was the BAD deviation index (BAD–D), with an AUC of 1.000 (sensitivity 100%; specificity 98.5%). This parameter derives from a combination of anterior and posterior elevation along with pachymetry distribution indices, and is calculated based on linear regression analysis. In the

Table 4: Pair-wise comparison of the AUC for elevation-derived parameters

	Ele B BFS 8 mm		*Ele B BFTE 8 mm*			*Ele F BFS 8 mm*			*Ele F BFTE 8 mm*		
	Max. 4 mm zone	*Thinnest*	*Apex*	*Max. 4 mm zone*	*Thinnest*	*Apex*	*Max. 4 mm zone*	*Thinnest*	*Apex*	*Max. 4 mm zone*	*Thinnest*
Ele B BFS 8 mm apex	<0.001	<0.001	0.785	<0.001	<0.001	0.32	<0.001	<0.001	0.986	<0.001	<0.001
Ele B BFS 8 mm max 4 mm zone		0.371	<0.001	0.689	0.212	<0.001	0.066	0.823	<0.001	0.065	0.475
Ele B BFS 8 mm thinnest			<0.001	0.226	0.378	<0.001	0.023	0.313	<0.001	0.008	0.104
Ele B BFTE 8 mm apex				<0.001	<0.001	0.396	<0.001	<0.001	0.873	<0.001	<0.001
Ele B BFTE 8 mm max 4 mm zone					0.081	<0.001	0.213	0.882	<0.001	0.112	0.691
Ele B BFTE 8 mm thinnest						<0.001	0.011	0.138	<0.001	0.003	0.035
Ele F BFS 8 mm apex							<0.001	<0.001	0.081	<0.001	<0.001
Ele F BFS 8 mm max 4 mm zone								0.151	<0.001	0.784	0.419
Ele F BFS 8 mm thinnest									<0.001	0.086	0.486
Ele F BFTE 8 mm apex										<0.001	<0.001
Ele F BFTE 8 mm max 4 mm zone											0.231

Ele F BFS 8 mm apex: Front surface elevation at the apex using the 8 mm best-fit sphere; Ele F BFS 8 mm max. 4 mm zone: Front surface elevation at the point with highest value within the 4 mm (diameter) zone centered at the apex using the 8 mm best-fit sphere; Ele F BFS 8 mm thinnest: Front surface elevation at the thinnest point using the 8 mm best-fit sphere; Ele B BFS 8 mm apex: Back surface elevation at the apex using the 8 mm best-fit sphere; Ele B BFS 8 mm max 4 mm zone: Back surface elevation at the point with highest value within the 4 mm (diameter) zone centered at the apex using the 8 mm best-fit sphere; Ele B BFS 8 mm thinnest: Back surface elevation at the thinnest point using the 8 mm best-fit sphere; Ele F BFTE 8 mm apex: Front surface elevation at the apex using the 8 mm best-fit toric ellipsoid; Ele F BFTE 8 mm max 4 mm zone: Front surface elevation at the point with highest value within the 4 mm (diameter) zone centered at the apex using the 8 mm best-fit toric ellipsoid; Ele F BFTE 8 mm thinnest: Front surface elevation at the thinnest point using the 8 mm best-fit toric ellipsoid; Ele B BFTE 8 mm apex: Back surface elevation at the apex using the 8 mm best-fit toric ellipsoid; Ele B BFTE 8 mm max 4 mm zone: Back surface elevation at the point with highest value within the 4 mm (diameter) zone centered at the apex using the 8 mm best-fit toric ellipsoid; Ele B BFTE 8 mm thinnest: Back surface elevation at the thinnest point using the 8 mm best-fit toric ellipsoid; De Long method

Table 6: Pair-wise comparison of the AUC for BAD-D and its derived indices

	BAD-Dam	*BAD-Db*	*BAD-De*	*BAD-Df*	*BAD-Dk*	*BAD-Dp*	*BAD-Dr*	*BAD-Dt*	*BAD-Dy*	*BAD-D*
BAD Daa	0.81	0.001	0.032	0.001	0.003	0.139	<0.001	<0.001	<0.001	0.29
BAD Dam		0.002	0.035	0.001	0.003	0.349	<0.001	<0.001	<0.001	0.275
BAD Db			0.053	0.934	0.638	0.003	<0.001	0.162	<0.001	<0.001
BAD De				0.108	0.273	0.078	<0.001	0.007	<0.001	0.009
BAD Df					0.581	0.003	<0.001	0.202	<0.001	<0.001
BAD Dk						0.007	<0.001	0.079	<0.001	0.001
BAD Dp							<0.001	<0.001	<0.001	0.129
BAD Dr								0.001	<0.001	<0.001
BAD Dt									<0.001	<0.001
BAD Dy										<0.001

BAD Df: Deviation of front elevation difference map; BAD Db: Deviation of front elevation difference map; BAD Dp: Deviation of average pachymetric progression; BAD Dt: Deviation of minimum thickness; BAD Dy: Deviation from the vertical displacement of the thinnest point from the apex; BAD De: Deviation from the posterior elevation at the thinnest point considering BFS 8 mm; BAD Dam: Deviation of ART max; BAD Daa: Deviation of ART avg; BAD Dk: Deviation from K_{max}; BAD Dr: Deviation from the more negative value on the relative thickness map; BAD D: Belin/Ambrósio enhanced ectasia total deviation value; De Long method

Table 7: Pair-wise comparison of the AUC for the the best topometric, tomographic and combined parameters

	Ele B BFS 8 mm thinnest	*Ele B BFTE 8 mm thinnest*	*ART max*	*ART avg*	*BAD-D*
ISV	0.504	0.277	0.012	0.01	0.003
Ele B BFS 8 mm thinnest		0.378	0.034	0.031	0.009
Ele B BFTE 8 mm thinnest			0.081	0.073	0.023
ART max				0.796	0.235
ART avg					0.247

ISV: Index of surface variance; Ele B BFS 8 mm thinnest: Back surface elevation at the thinnest point using the 8 mm best-fit sphere; Ele B BFTE 8 mm thinnest: Back surface elevation at the thinnest point using the 8 mm best-fit toric ellipsoid; ART max: Ambrósio relational thickness maximum; ART avg: Ambrósio relational thickness average; BAD D: Belin/Ambrósio enhanced ectasia total deviation value; De Long method

pairwise comparisons of the AUC for BAD-D and its derived indices, there was no statistically difference for BAD-Daa, BAD-Dam and BAD-Dp ($p > 0.05$). Such indices are derived from relation thickness and posterior elevation data. In this study, the cutoff for BAD-D parameter was set at >1.34. At Belin and Ambrosio Display, this parameter turns yellow only when is > 1.60, leading to possibles misinterpretation of the examination.

This study displays the best cutoffs with optimal sensitivity and specificity of topometric and tomographic parameters to diagnose keratoconus. Both indices demonstrated to be accurate for distinguishing normal corneas and those with keratoconus. Front surface curvature-derived indices may be used as objective parameters to detect keratoconus, but can be normal in mild forms of ectasia without front surface changes. This can lead to relatively later identification of ectasia with lower sensitivity than tomographic indices based on posterior elevation and pachymetric distribution. In this study, the KC study population required bilateral disease with eyes meeting standard CLEK diagnostic criteria which are predominantly based on keratometric and anterior curvature parameters. It would be expected that topometric parameters would not perform as well in earlier disease.

Combined tomographic parameters, such as BAD-D, ART avg and ART max, are excellent tools that provide an enhanced approach for detecting early forms keratoconus. Future studies are necessary to test the sensitivity of these parameters to detect milder forms of ectasia when assessing the risk of developing ectasia after LASIK. Further understanding of corneal biomechanics and its correlation to these parameters may further improve the detection of mild forms of keratoconus.[28]

REFERENCES

1. Krachmer JH, Feder RS, Belin MW. Keratoconus and related noninflammatory corneal thinning disorders. Surv Ophthalmol 1984;28(4):293-322.
2. Rabinowitz YS. Keratoconus. Surv Ophthalmol 1998;42(4):297-319.
3. Amsler M. The 'forme fruste' of keratoconus. Wien Klin Wochenschr 1961;73:842-43.
4. Klyce SD. Computer-assisted corneal topography. High-resolution graphic presentation and analysis of keratoscopy. Invest Ophthalmol Vis Sci 1984;25(12):1426-35.
5. Wilson SE, Lin DT, Klyce SD. Corneal topography of keratoconus. Cornea 1991;10(1):2-8.
6. Maeda N, Klyce SD, Tano Y. Detection and classification of mild irregular astigmatism in patients with good visual acuity. Surv Ophthalmol 1998;43(1):53-58.

7. Rabinowitz YS, McDonnell PJ. Computer-assisted corneal topography in keratoconus. Refract Corneal Surg 1989;5(6): 400-08.
8. Holladay JT. Keratoconus detection using corneal topography. J Refract Surg 2009;25(10 Suppl):S958-62.
9. Maeda N, Klyce SD, Smolek MK, Thompson HW. Automated keratoconus screening with corneal topography analysis. Invest Ophthalmol Vis Sci 1994;35(6):2749-57.
10. Ambrosio R Jr, Klyce SD, Wilson SE. Corneal topographic and pachymetric screening of keratorefractive patients. J Refract Surg 2003;19(1):24-29.
11. Oshika T, Klyce SD. Corneal topography in LASIK. Semin Ophthalmol 1998;13(2):64-70.
12. Ambrosio R Jr., Wilson SE. Complications of laser in situ keratomileusis: Etiology, prevention and treatment. J Refract Surg 2001;17(3):350-79.
13. Randleman JB, Woodward M, Lynn MJ, Stulting RD. Risk assessment for ectasia after corneal refractive surgery. Ophthalmology 2008;115(1):37-50.
14. Binder PS, Trattler WB. Evaluation of a risk factor scoring system for corneal ectasia after LASIK in eyes with normal topography. J Refract Surg 2010;26(4):241-50.
15. Ambrosio R Jr., Belin MW. Imaging of the cornea: Topography vs tomography. J Refract Surg 2010;26(11):847-49.
16. Belin MW, Khachikian SS, McGhee CN, Patel D. New technology in corneal imaging. Int Ophthalmol Clin 2010;50(3):177-89.
17. Salomao MQ, Esposito A, Dupps WJ Jr. Advances in anterior segment imaging and analysis. Curr Opin Ophthalmol 2009;20(4):324-32.
18. Reinstein DZ, Gobbe M, Archer TJ, Silverman RH, Coleman DJ. Epithelial, stromal, and total corneal thickness in keratoconus: Three-dimensional display with artemis very-high frequency digital ultrasound. J Refract Surg 2010;26(4):259-71.
19. Reinstein DZ, Archer TJ, Gobbe M, Silverman RH, Coleman DJ. Repeatability of layered corneal pachymetry with the artemis very high-frequency digital ultrasound arc-scanner. J Refract Surg 2010;26(9):646-59.
20. Huang D. A reliable corneal tomography system is still needed. Ophthalmology 2003;110(3):455-56.
21. Luz A, Ursulio M, Castaneda D, Ambrosio R Jr. Corneal thickness progression from the thinnest point to the limbus: Study based on a normal and a keratoconus population to create reference values. Arquivos Brasileiros de Oftalmologia 2006;69(4):579-83.
22. Ambrosio R Jr, Alonso RS, Luz A, Coca Velarde LG. Corneal-thickness spatial profile and corneal-volume distribution: Tomographic indices to detect keratoconus. J Cataract Refract Surg 2006;32(11):1851-59.
23. Ambrosio R Jr, Caiado AL, Guerra FP, Louzada R, Roy AS, Luz A, et al. Novel pachymetric parameters based on corneal tomography for diagnosing keratoconus. J Refract Surg 2011;27(10):753-58.
24. Belin MW, Khachikian SS. An introduction to understanding elevation-based topography: How elevation data are displayed – a review. Clin Experiment Ophthalmol 2009;37(1):14-29.
25. Wagner H, Barr JT, Zadnik K. Collaborative longitudinal evaluation of keratoconus (CLEK) study: Methods and findings to date. Cont Lens Anterior Eye 2007;30(4):223-32.
26. Krumeich JH, Daniel J, Knulle A. Live-epikeratophakia for keratoconus. J Cataract Refract Surg 1998;24(4):456-63.
27. Ambrosio R Jr, Dawson DG, Salomao M, Guerra FP, Caiado AL, Belin MW. Corneal ectasia after LASIK despite low preoperative risk: tomographic and biomechanical findings in the unoperated, stable, fellow eye. J Refract Surg 2010;26(11): 906-11.
28. Ambrosio R Jr, Nogueira LP, Caldas DL, Fontes BM, Luz A, Cazal JO, et al. Evaluation of corneal shape and biomechanics before LASIK. Int Ophthalmol Clin 2011;51(2):11-38.
29. Belin MW, Ambrosio R Jr. Corneal ectasia risk score: Statistical validity and clinical relevance. J Refract Surg 2010;26(4): 238-40.
30. Khachikian SS, Belin MW. Posterior elevation in keratoconus. Ophthalmology 2009;116(4):816-17.

ABOUT THE AUTHORS

Fernando Faria Correia

Resident, Department of Ophthalmology, Centro Hospitalar São João Portugal, Research Associate, Rio de Janeiro Corneal Tomography and Biomechanics Study Group, Brazil

Isaac Ramos

Research Associate, Rio de Janeiro Corneal Tomography and Biomechanics Study Group, Brazil

Bernardo Lopes

Research Associate, Rio de Janeiro Corneal Tomography and Biomechanics Study Group, Brazil

Marcella Q Salomão

Research Associate, Rio de Janeiro Corneal Tomography and Biomechanics Study Group, Brazil

Allan Luz

Doctorate PhD Fellow, Department of Ophthalmology, UNIFESP (Universidade Federal de São Paulo), Research Associate, Rio de Janeiro Corneal Tomography and Biomechanics Study Group, Brazil

Rosane O Correa

Research Associate, Rio de Janeiro Corneal Tomography and Biomechanics Study Group, Brazil

Michael W Belin

Professor, Department of Cornea/Refractive and Ophthalmology University of Arizona, USA

Renato Ambrósio Jr (Corresponding Author)

Associate Professor, Department of Ophthalmology, UNIFESP (Universidade Federal de São Paulo), Founder and Scientific Director Rio de Janeiro Corneal Tomography and Biomechanics Study Group Brazil, e-mail: dr.renatoambrosio@gmail.com